AGU PUBLICATIONS

Geophysical Research Letters

RESEARCH LETTER
10.1002/2016GL070357

**Key Points:**
- Scale-dependent triplet statistics are computed from two launches of ~90 surface drifter triads with initial 100 m and 500 m sides
- Unlike AVISO-based trajectories, drifter triangles reach highly elongated configurations on short (12 h-2 day) timescales
- Magnitudes of triplet-derived strain rate and divergence are scale dependent and comparable and exceed the local Coriolis parameter

**Supporting Information:**
- Supporting Information S1

**Correspondence to:**
M. Berta,
maristella.berta@sp.ismar.cnr.it

**Citation:**
Berta, M., A. Griffa, T. M. Özgökmen, and A. C. Poje (2016), Submesoscale evolution of surface drifter triads in the Gulf of Mexico, *Geophys. Res. Lett.*, *43*, 11,751–11,759, doi:10.1002/2016GL070357.

Received 7 JUL 2016
Accepted 22 OCT 2016
Accepted article online 28 OCT 2016
Published online 19 NOV 2016



# Submesoscale evolution of surface drifter triads in the Gulf of Mexico

**Maristella Berta[1], Annalisa Griffa[1], Tamay M. Özgökmen[2], and Andrew C. Poje[3]**

[1]CNR-ISMAR, La Spezia, Italy, [2]RSMAS, University of Miami, Coral Gables, Florida, USA, [3]Department of Mathematics, CUNY, New York, New York, USA

**Abstract** Triangle shape metrics are analyzed to quantify the evolution of submesoscale (100–500 m initial separation) surface drifter triplets released in the northern Gulf of Mexico. The observations are compared to synthetic drifters advected by geostrophic velocity fields derived from satellite altimetry. Observed submesoscale triads evolve rapidly, reaching highly elongated configurations on timescales of 6 h to 2 days, in contrast to 6 days or longer for altimetry-derived synthetic data. Estimates of horizontal divergence and strain rate from the drifter triplets indicate the relative importance of divergence in the evolution of triangle shape. Horizontal divergence is scale dependent, on the order of the local Coriolis parameter, and 2 to 3 times larger for initial 100 m scales compared to initial 500 m scales.

## 1. Introduction

Ocean transport problems are most naturally treated in the Lagrangian reference frame. Predicting the source location of observed debris in the case of airline accidents over marine waters [*Normile*, 2014] relies on the statistics of single trajectories, or absolute dispersion, with analysis methods dating back to *Taylor* [1921]. The fate of a rapid release of pollutants into the ocean by catastrophic accidents, such as radioactive materials in the case of the Fukushima meltdown [*Rypina et al.*, 2014], or hydrocarbons in marine oil spills, such as Deepwater Horizon (DWH) [*Crone and Tolstoy*, 2010], can be approached using two-particle statistics, or relative dispersion, studied since *Richardson* [1926].

However, without explicit assumptions about the statistical geometry of the advecting velocity field, neither absolute nor relative dispersion uniquely quantifies the evolution of the shape of surface tracer patches. The growth of a tracer patch constrained to move on the ocean surface is controlled by several mechanisms. Fluctuations of the horizontal velocity field on spatial scales commensurate with the size of the patch increase patch size through local, turbulent dispersion. Horizontal velocity gradients at larger scales induce shear dispersion. In contrast, owing to the two-dimensional compressibility of the surface velocity field [*Boffetta et al.*, 2004; *Cressman et al.*, 2004a; *Kalda et al.*, 2014], convergence zones act to arrest patch growth, possibly only along preferred directions.

Aspects of the geometry of the two-dimensional (2-D) surface dispersion can be quantified by simultaneous observations of $N \geq 3$ Lagrangian drifters [*Pumir et al.*, 2000; *Thiffeault*, 2005]. Drifter triplets are also the minimal configuration required for directly estimating velocity gradients and related kinematic properties [*Molinari and Kirwan*, 1975; *Magome et al.*, 2007]. Direct observations of surface drifter triads, especially at small spatial scales (order of 1 km or less), are sparingly rare in oceanography since they require specialized launch templates and large numbers of drifters to obtain reliable statistics. Here we exploit the triplet-based launch template used during the 2012 GLAD experiment [*Poje et al.*, 2014] to investigate the evolution of surface tracer patches.

The evolution of triangles in 2-D nondivergent flows has been studied numerically and experimentally in time-dependent laminar (chaotic) flows [*Merrifield et al.*, 2010; *de Chaumont Quitry et al.*, 2011] and turbulent flows [*Pumir et al.*, 2000; *Biferale et al.*, 2005]. Consider initially equilateral triangles with sides $l_1 = l_2 = l_3$, and renormalized "radius of gyration," $R^2 = \frac{1}{3}(l_1^2 + l_2^2 + l_3^2)$, as previously defined by *de Chaumont Quitry et al.* [2011]. For $R \ll L$, where $L$ is the scale of coherent eddies in the underlying flow, triangles have an initial phase of strong distortion leading toward collinearity, due to the hyperbolicity in the flow. As $R$ increases, particles sample different flow structures. Triangles continue to elongate with one side typically becoming much shorter than the other two. When $R > L$, the motion of all three particles is uncorrelated, and triangles evolve toward a noncollinear, isotropic shape in this diffusive limit.

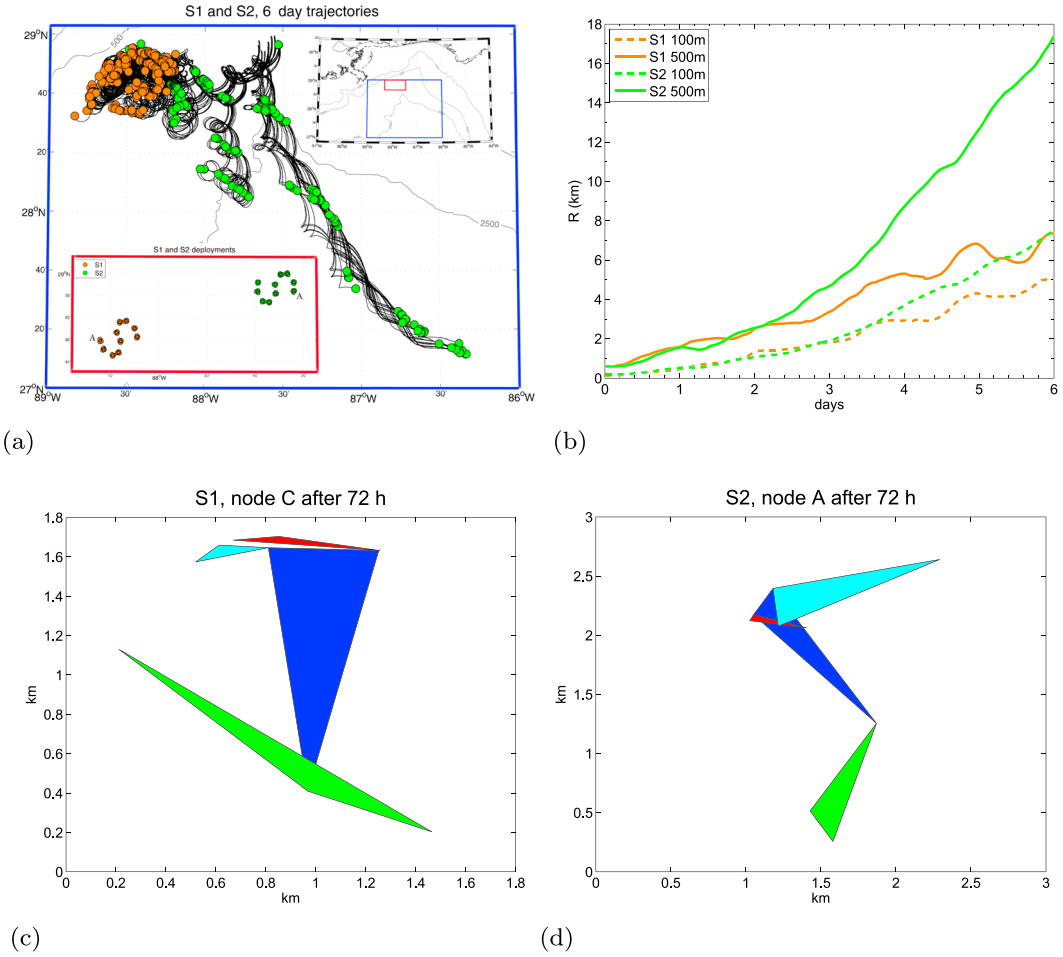


**Figure 1.** (a) *S1* (orange) and *S2* (green) 6 day trajectories (dots every 2 days). Embedded on the right: the area of deployment. Embedded on the left: *S1* and *S2* deployment configuration (each circle indicates a nine-drifter node). Letter *A* indicates the first deployed node for each *S*. (b) Radius of gyration for triplets in *S1* and *S2*. (c and d) Triplet configuration for single nodes in *S1* and *S2* after 3 days. In each, the dark blue triangle corresponds to *T*500 triplet.

In 2-D divergent flows, such as those advecting buoyant tracers at the ocean's surface (e.g., oil and drifters), the picture is modified due to the clustering and trapping of particles in convergence zones [*Falkovich et al.*, 2001; *Cressman et al.*, 2004a]. Clustering acts to reduce dispersion and increase the tendency of triangles to remain elongated for long times, delaying and possibly inhibiting transition toward the diffusive limit [*Boffetta et al.*, 2004; *Cressman et al.*, 2004a, 2004b].

In the present study, triplet shape metrics from in situ drifters are analyzed to further quantify tracer patch evolution, complementing prior numerical investigations on surface clustering [*Zhong and Bracco*, 2013; *Kalda et al.*, 2014; *Huntley et al.*, 2015; *Jacobs et al.*, 2016] and ultimately informing oil spill mitigation efforts. *LaCasce and Ohlmann* [2003] and *LaCasce* [2008] investigated triangle evolution from 30 chance triplets of drifters initially separated by ≈1 km in the Gulf of Mexico. While there were indications of an initial stretching phase, consistent with observed two point statistics, the 1 km drifter position accuracy precluded a detailed study of shape evolution at early times. Aspect ratio (height to base) results for larger 5 km pairs did suggest considerable initial elongation of these triangles followed by a diffusive tendency toward a more isotropic shape.

Traditional data constraints on drifter triad availability and temporal sampling have been recently overcome by a particular launch strategy of large numbers of GPS-tracked drifters during the GLAD (Grand LAgrangian Deployment) expedition in the northern Gulf of Mexico. We concentrate on the first 3–6 days of triad deformation, during which separation scales are of the order of 100 m to 10 km. While now readily observed in high-resolution satellite imagery, direct in situ measurement of submesoscale fields remains challenging

[*Shcherbina et al.*, 2013; *Poje et al.*, 2014] given the inherent aliasing issues associated with relatively rapid temporal variation (hourly timescales) of relatively large (1–10 km) spatial structures. Drifters were released in the area influenced by the Mississippi river outflow and were grouped in two main launches, *S*1 and *S*2 (Figure 1a), each one consisting of approximately 30 triangles of 100 m side and 30 of 500 m side. *S*2 drifters were launched across a strong density front in a high strain mesoscale area [*Olascoaga et al.*, 2013], and most were entrained in a frontal region with southwestward flow. *S*1 drifters, on the other hand, were launched in an area with weaker density gradients. Here we compare observations with synthetic trajectories produced by altimetry (AVISO) based velocity fields [*Rio*, 2010; *Olascoaga et al.*, 2013] starting from the same initial positions as the in situ drifters. Given that AVISO only resolves mesoscale features and geostrophy only captures the nondivergent component of the flow, differences between AVISO and drifter triplets are expected to highlight the effects of local, ageostrophic/submesoscale components of the surface flow field.

The main goals of the study are (i) to compare statistics of initial triangle shape evolution from *S*1 and *S*2 drifters with each other and with those derived from AVISO fields and (ii) to examine drifter-based strain rate and divergence statistics influencing shape evolution.

## 2. Data Sets

The GLAD drifter experiment took place in 17–31 July 2012 in the area of the DWH spill in the DeSoto Canyon (data set publicly available online [*Özgökmen*, 2012]). During GLAD, about 300 CODE (Coastal Ocean Dynamics Experiment) surface drifters, designed to follow the average currents over the top 1 m of the ocean with errors of 0.01 to 0.03 m/s for winds up to 10 m/s [*Davis*, 1985; *Poulain et al.*, 2009], were deployed. The GPS units installed in the drifters transmitted their position every 5 min with a root-mean-square error of 6 m. The trajectories were filtered using an acceleration-based filter with velocity/position information provided at uniform 15 min intervals [*Yaremchuk and Coelho*, 2014]. Following *Olascoaga et al.* [2013] and *Berta et al.* [2015], synthetic drifters are also computed using AVISO altimetry. Satellite-derived velocity data are available on a 1/10° mesh updated at 24 h intervals.

Here we focus on two main launches, denoted *S*1 and *S*2, of 89 and 90 drifters, respectively. Each *S* launch consisted of 10 nodes of nine drifters arranged in a nested, space-filling configuration over an area of ~8 km × 10 km (Figure 1a and Figure SM1 in the supporting information). Each nine-drifter node was comprised of three triplets launched as approximately equilateral triangles with nominal 100 m sides (denoted *T*100). These three triplets were deployed at 500 m distance from each other [*Poje et al.*, 2014] resulting in 30 original *T*100 triangles in *S*2, 29 in *S*1, and the same number of 500 m side triangles (denoted *T*500) formed by subsampling a unique drifter in each *T*100 triplet. Drifter trajectories during the first 6 days show the different fate of the two launches (Figure 1a). Strong inertial oscillations are visible in the trajectories, as expected due to shallow mixed layers in the summer season [*Mariano et al.*, 2016]. The triplet gyration radius, *R*, increases in time (Figure 1b) in a similar way for *S*1 and *S*2 for values up to $R \approx 3$ km. At larger distances, *S*2 triplets, especially the larger ones in *T*500, grow more quickly. Examples of triangle shapes within a node, a single *T*500 and three *T*100, 3 days after launch are shown in Figures 1c and 1d. In these examples, *T*100 and *T*500 triangles in *S*2 deform and elongate in a qualitatively similar way, while for *S*1, *T*100 triangles are preferentially elongated compared to the initial 500 m triangle.

## 3. Metrics of Triad Shape Analysis

The evolution of triangle shape is quantified using two metrics. The first one is the scaled ratio between the triangle area, *A*, and the square of the triangle perimeter, *P*,

$$\Lambda(t) = \beta A(t)/P(t)^2 = \frac{\beta\sqrt{p(p-l_1)(p-l_2)(p-l_3)}}{(l_1+l_2+l_3)^2}, \quad (1)$$

where $p = P/2$, and $\beta = 36/\sqrt{3}$ is chosen such that $\Lambda = 1$ for equilateral triangles [see *Pumir et al.*, 2000; *Castiglione and Pumir*, 2001]. Since $\Lambda \to 0$ for collinear arrangements, the metric provides a size independent assessment of the tendency of the underlying flow to elongate surface patches.

The second metric is based on the fact that self-similar triangle shape, independent of size and orientation, can be uniquely defined by two quantities. Several shape metrics have been proposed in the literature

[e.g., *Pumir et al.*, 2000; *Cressman et al.*, 2004a]. Here following *Merrifield et al.* [2010] and *de Chaumont Quitry et al.* [2011], we use a two-parameter metric that has an intuitive interpretation for the case of triangles. We track shape evolution in $(\theta, \gamma)$ space, where $\theta$ is the largest internal angle of the triangle (ranging from $\pi/3$ for equilateral triangles to $\pi$ for collinear vertices) and $\gamma$ is the ratio of smallest to intermediate triangle sides (varying between 0 and 1). For small $\gamma$, two of the drifters are much closer to each other than the third, while $\gamma = 1$ corresponds to equidistant drifters. Examples of self-similar triangle shapes for various values of $(\hat{\theta} = \theta/\pi, \gamma)$ are shown in Figure 2. Geometry constrains configurations such that $\gamma \geq 1 - 2\theta/\pi$.

## 4. Results on Drifter Triad Shape Statistics

The time evolution of the average $\Lambda(t)$ (line) and its standard deviation (shaded) are shown in Figure 3 for a period of 6 days, during which the number of triplets remains constant. In both launches, $\Lambda(0)$ is smaller than one, due to deformation during the time between launching the first and last drifters in any single triplet. Drifter observations for *S*2 (Figures 3a and 3b, black lines) show consistent elongation of triads with convergence toward $\Lambda \approx 0.2$ during the first 2 days (more quickly for the *T*500 set). $\Lambda(t)$ computed from AVISO trajectories evolves on significantly slower timescales with elongation appreciably less than that of the observations in the 6-day window.

Similar results hold for *S*1 (Figures 3c and 3d) with AVISO-based triplets showing significantly less elongation at initial times than the observed drifter triplets for both *T*100 and *T*500. GLAD *S*1 drifters at both 100 m and 500 m separations indicate extremely rapid decrease in $\Lambda$ values during the first 12 h. Unlike the *S*2 launch, where both *T*100 and *T*500 triads attain approximately equal minimum $\Lambda$ values, the *S*1 observations indicate that the smaller triangles reach more elongated shapes, on average, than those initially separated by 500 m. Convergence of $\Lambda$ curves from AVISO and *S*1 estimates after 6 days provides an estimate for the time scale required for mesoscale straining. The much slower evolution of $\Lambda(t)$ in the AVISO-based results supports the idea that submesoscale/ageostrophic motions not resolved by the altimeter data control the deformation of surface tracer patches for times shorter than 6 days.

Compared to the analysis based on two-particle statistics of the same data set by *Poje et al.* [2014], which shows that scale-dependent relative dispersion is very similar for both *S*1 and *S*2 [*Poje et al.*, 2014, Figure 5] (Figure 1b), the timescales and evolution of three-point metrics are markedly different in the two samples. The behavior of *S*1 triplets are more scale dependent with *T*100 triangles distorting faster, and more, than the *T*500 ones (Figure 3). Unlike *S*2, where the smaller triangles actually evolve slightly slower than the larger ones, the scale dependence in *S*1 is consistent with triplet statistics in 2-D turbulence [*Pumir et al.*, 2000]. In both *S*1 and *S*2, however, there is no tendency for $\Lambda(t)$ to relax back toward higher values consistent with Gaussian statistics. In this sense, the behavior of $\Lambda(t)$ in both *S*1 and *S*2 is more consistent with compressible surface turbulence results [e.g., *Cressman et al.*, 2004a], where surface convergence zones act to maintain elongation in the presence of fluctuations.

Given the rapid distortion seen in $\Lambda(t)$, the analysis of evolution in $(\hat{\theta}, \gamma)$ space is focused on the initial 3 day period after launch. During this time, the average triangle size *R* for *T*500 triangles increases from 0.5 to ~4 km and for *T*100 triangles from 0.1 to ~2 km (see Figure 1b). Average initial configurations (stars) and trajectories in the phase space are shown in Figures 2a, 2c, and 2e, superimposed on corresponding images of triangles at various locations. For reference, the diffusive limit, numerically determined for simple Brownian motion [*de Chaumont Quitry et al.*, 2011], is given as a black dot at $(\hat{\theta} = 0.65, \gamma = 0.55)$. Figures 2b, 2d, and 2f show examples of individual triplet configurations (dots), sampled every 2 h, in selected nodes representative of the overall distribution (see supporting information Figure SM2).

The AVISO *S*1 results in Figures 2a and 2b provide a reference case where shape deformation is driven only by mesoscale fields (similar results hold for *S*2, not shown). Changes in triangle shape are relatively small during the 3 days of analysis, consistent with AVISO elongation timescales shown in Figure 3. Average trajectories and individual triplet starting as equilateral configuration remain confined in the upper left quadrant of the phase space away from regions of highly distorted triangle shape. Consistently, individual triplets starting with elongated shape persist in their initial configuration.

In contrast, GLAD *S*2 observations (Figures 2c and 2d), for both *T*100 and *T*500 average trajectories, rapidly evolve toward collinear states with $\hat{\theta} \approx 0.9$ and values of $\gamma \approx 0.3$. This is shown also by the examples of triplet configurations that tend toward regions of high $\hat{\theta}$ and small $\gamma$. The similarity between *T*100 and *T*500 suggests

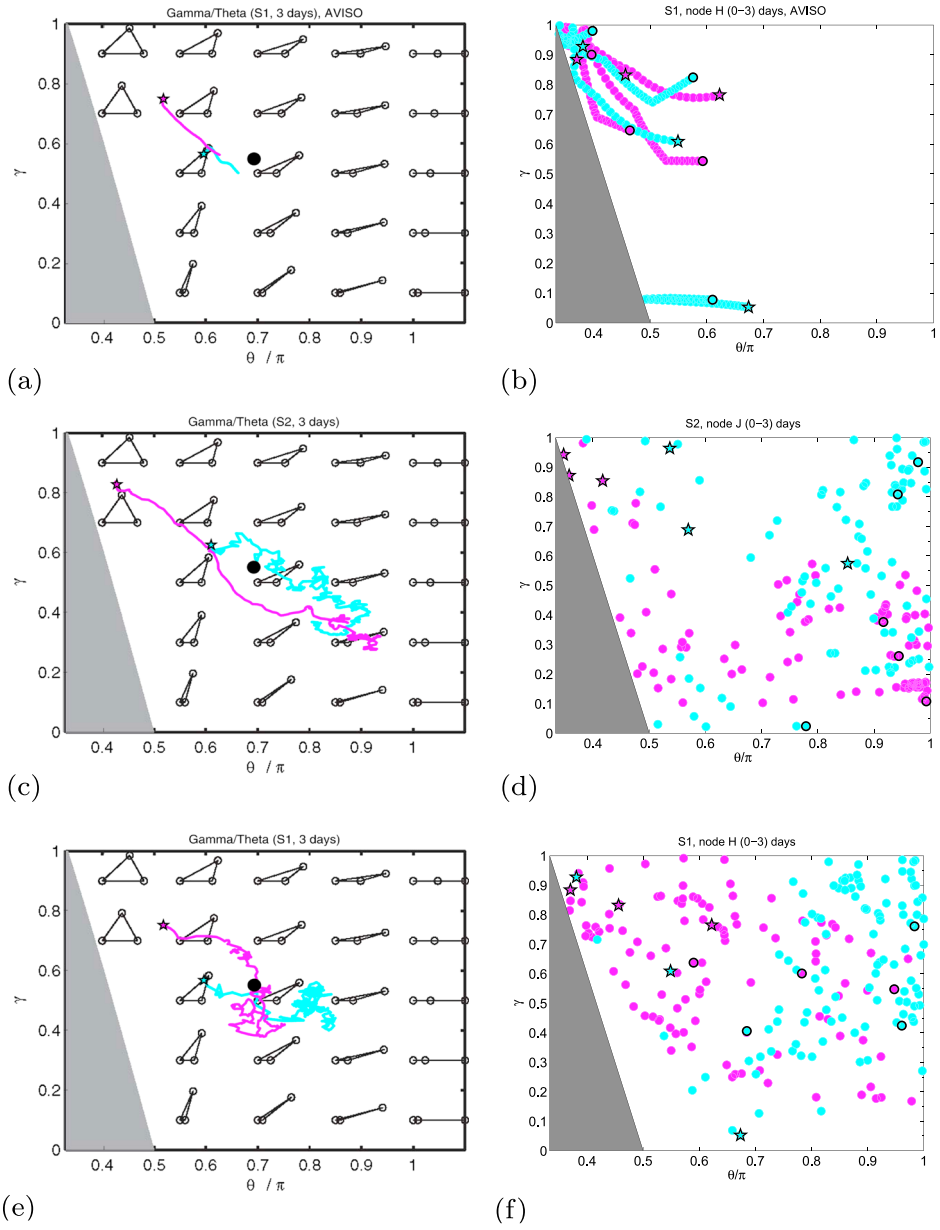


**Figure 2.** Statistics of triangle shape in the $(\hat{\theta}, \gamma)$ space for (a and b) AVISO *S*1, (c and d) *S*2 drifters, and (e and f) *S*1 drifters for the first 3 days. Figures 2a, 2c, and 2e show average trajectories superimposed on examples of triangle shapes (modified from *Merrifield et al.* [2010]). Black dots in Figures 2a, 2c, and 2e represent the diffusive limit. Figures 2b, 2d, and 2f show triplet configurations (dots) for selected nodes of AVISO and drifters *S*2 and *S*1. Initial configurations are denoted by black stars, while final configurations are represented by black circles. Cyan and magenta indicate *T*100 and *T*500, respectively. Triangles are not defined in the gray wedge.

that both sets sample spatial scales smaller than the local flow scale [*de Chaumont Quitry et al.*, 2011], namely, $R < L$ and thus $L > 500$ m.

For GLAD *S*1 (Figures 2e and 2f), the average *T*100 trajectory tends toward elongation (maximum $\hat{\theta} \approx 0.85$) consistent with observations from *S*2. On the other hand, *S*1 *T*500 triads show smaller deformation over similar times with $\hat{\theta}$ values of $\approx 0.7$. The distribution of individual triplets in the configuration space is markedly different for the two sets, with *T*100 moving toward high elongation areas with $\gamma$ generally greater than 0.4. The larger *T*500 triads show less elongation, remaining mostly concentrated in the left half of the phase space (see also Figure SM2).

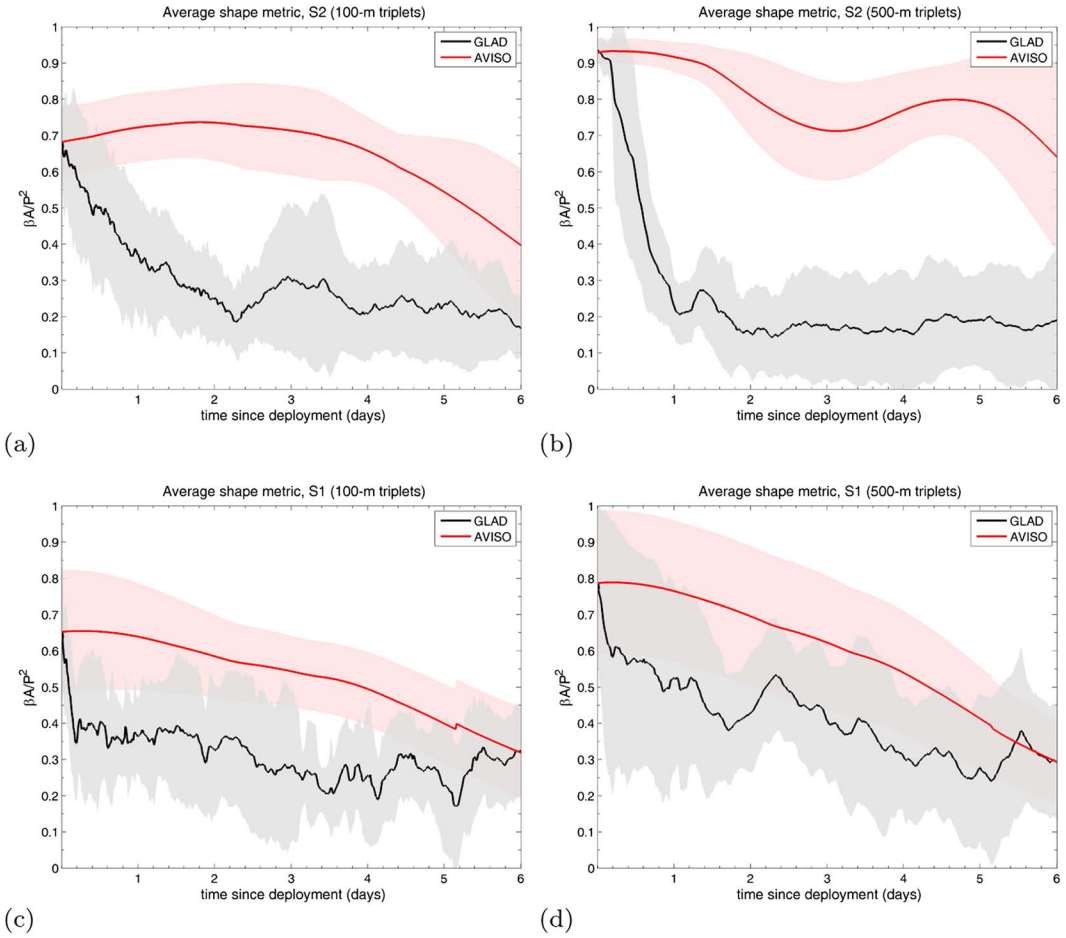


**Figure 3.** Time series of $\Lambda$ average (lines) and standard deviation (shading) for drifters (black) and AVISO trajectories (red). Results for (a and b) *S*2, (c and d) for *S*1. *T*100 is represented in Figures 3a and 3c, while *T*500 is represented in Figures 3b and 3d.

To summarize, for GLAD *S*2, both *T*100 and *T*500 curves cover the same region of phase space and converge to maximum elongation angles. A majority of *T*500 triangles evolve toward low $\gamma$ configurations, while *T*100 triangles show a bimodal distribution of $\gamma$ values (see also Figure SM2). For *S*1, *T*100 triangles converge to maximum $\theta$, while slower evolution is observed in the *T*500 triangles. Also, in comparison to *S*2, there is less tendency to form triangles with $\gamma < 0.5$, especially for the initially larger triplets *T*500. The difference between the evolution of *T*100 and *T*500 triads in *S*1 suggests significant contributions from intermediate scales, $L <$ 500 m, which preferentially influence the evolution of *T*100 triangles. These observations are consistent with those shown in Figures 1c, 1d, and 3.

## 5. Drifter-Based Estimation of Strain Rate and Divergence

Strain rate and divergence play an important role in tracer patch deformation [*Gawędzki and Vergassola*, 2000; *Boffetta et al.*, 2004; *Kalda et al.*, 2014; *Huntley et al.*, 2015]. Here we provide estimates of these kinematic, velocity gradient properties from the drifters. On the basis of the pioneering work by *Molinari and Kirwan* [1975], triangles allow estimation of divergence and strain rate, unlike single- and two-particle statistics. Thus, triplet-based estimates are valid as long as triplets maintain noncollinear arrangements, while they deteriorate as triangles elongate.

We estimate horizontal divergence $\delta = u_x + v_y$ and strain rate $\alpha = (N^2 + S^2)^{1/2}$, with $N = u_x - v_y$; $S = v_x + u_y$, directly from the drifter triangle evolution. Here $u$ and $v$ are zonal and meridional velocity components, the subscripts $x$ and $y$ indicate zonal and meridional partial derivatives, and $N$ and $S$ are the stretching and shearing components of the strain rate, respectively.

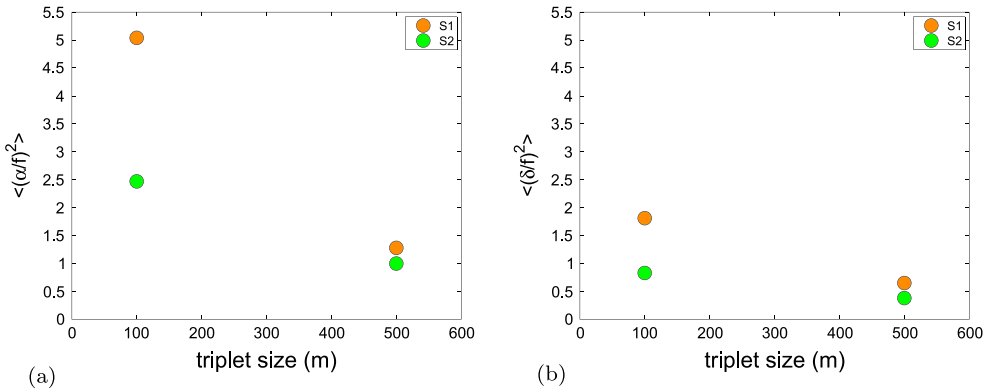


**Figure 4.** Scale dependence of mean square (a) strain rate and (b) divergence, normalized by $f$ during the initial 12 h of deployment.

The method based on the area change rate is used to compute the kinematic quantities following *Molinari and Kirwan* [1975], *Magome et al.* [2007], and *LaCasce* [2008], considering only noncollinear triplets during the first 12 h of evolution. For $\delta$, the computation is directly based on the fact that horizontal divergence can be expressed as the fractional time rate of change of the horizontal area $A$ of a triangle, while for $N$ and $S$ appropriate rotations of the velocity vectors are performed [*Saucier*, 1955] that allow writing them in an analogous form. The details of the computation and the results of an extensive sensitivity analysis are provided in the supporting information (Text SM1).

The normalized distributions of $\delta/f$ and $\alpha/f$ (where $f$ is the Coriolis parameter) are computed for the four data sets given by $T100$ and $T500$ for $S1$ and $S2$. Probability distributions and main statistics are shown in the supporting information (Figure SM3). In Figure 4, we present the mean square values for divergence and strain rate, $< (\delta/f)^2 >$ and $< (\alpha/f)^2 >$, respectively. We find that both quantities are scale dependent, namely, there is more strain rate as well as divergence at 100 m triad scales than at 500 m scales. Consistent with the previous triplet metrics, it can be also seen from Figure 4 that the $S1$ release is more scale dependent than the $S2$ release, pointing toward inhomogeneity in the triad kinematics within DeSoto Canyon, despite proximity of these two drifter data sets in space and time.

As a simple measure of the relative size of $\delta/f$ and $\alpha/f$ in the four data sets, we compute the ratio of the mean square values of divergence and strain rate, $\hat{C} = < (\delta/f)^2 > / < (\alpha/f)^2 >$. For $S2$ $T100$, $S2$ $T500$, and $S1$ $T100$, $\hat{C} \approx 0.35$, while for $S1$ $T500$, $\hat{C} \approx 0.5$. In $S1$, the average strain rate is reduced by a factor of $\approx 4$ as the triangle size increases from $T100$ to $T500$ (Figure 4). In contrast, $\alpha$ for $S2$ decreases considerably less. This is consistent with the notion that the distortion of $S1$ triangles is affected by local straining at intermediate scales, $L < 500$ m. For both $S1$ and $S2$, the divergence computed from smaller triplets, $T100$, is $\sim 2-3$ times larger than that observed for $T500$ triplets.

## 6. Summary and Discussion

Two distinct sets ($S1$ and $S2$) of 90 GLAD drifter triplets, launched with nominal side lengths of 100 m and 500 m, are used to estimate the statistics of initial triangle shape evolution in the DeSoto Canyon region.

In contrast to AVISO-based triplets which show a similar, slow, evolution of shape metrics for 100 and 500 m triplets, the drifter data, especially for the $S1$ launch, show distinct scale dependence. This supports the view that local dynamics, as opposed to nonlocal mesoscale-driven dynamics, dominate triplet evolution in the Canyon at least during the first several days. Unlike two-particle statistics which show minimal differences between $S1$ and $S2$ releases, three-particle metrics clearly distinguish the two releases and allow estimates of the relative strength of scale-dependent horizontal divergence and strain rate in the kinematics.

The $S2$ triplets, launched across a strong density gradient and flanking mesoscale fronts, show strong distortion and a tendency toward collinearity during the first 2 days. The similarity of triangle shape evolution for the $T100$ and $T500$ triangles is consistent with a dominant flow scale larger than the triangle size during the first 2 days after launch. The $S1$ triplets, which sampled the less energetic western part of the DeSoto Canyon, show different results for the $T100$ and $T500$ triangles with 100 m triangles evolving faster toward more elongated

shapes than 500 m triplets. These differences suggest the importance of local flow structures at intermediate scales, $L < 500$ m, that more effectively distort the smaller triplets in this region. The statistics of strain rate and horizontal divergence obtained from the triplets also indicate more significant scale dependence of velocity gradients in $S1$ than $S2$. In all cases, divergence is a significant fraction of the strain rate and clearly affects the evolution of drifter triads. Unlike incompressible 2-D turbulence simulations and experiments, where elongated triangles eventually return to more isotropic, Gaussian configurations [*Pumir et al.*, 2000], surface drifter triads show a strong tendency to persist in elongated states.

The results of this study show that launching massive arrays of drifters in geometrically configured, multiscale templates can be used to infer how patches of tracers of different sizes evolve under complex oceanic surface fields. The differences in elongation timescales (as quantified by the $\Lambda$ metric), in the degree of distortion (from $\gamma$-$\theta$ state space), and in the scale dependence of divergence and strain rate between the two drifter launches highlight the degree of inhomogeneity of surface flow fields in the Canyon.

**Acknowledgments**
This research paper, developed in the framework of CARTHE, was made possible by the grant from the Gulf of Mexico Research Initiative. Data are publicly available through the Gulf of Mexico Research Initiative Information and Data Cooperative (GRIIDC) at https://data.gulfresearchinitiative.org/data/R1.x134.073:0004, doi:10.7266/N7VD6WC8. The authors wish to express their gratitude to Simone Marini and Angelique Haza for discussions relevant to this paper.

## References

Berta, M., A. Griffa, M. G. Magaldi, T. M. Özgökmen, A. C. Poje, A. C. Haza, and M. J. Olascoaga (2015), Improved surface velocity and trajectory estimates in the Gulf of Mexico from blended satellite altimetry and drifter data, *J. Atmos. Oceanic Technol.*, *32*, 1880–1901, doi:10.1175/JTECH-D-14-00226.1.

Biferale, L., G. Boffetta, A. Celani, B. J. Devenish, A. Lanotte, and F. Toschi (2005), Multiparticle dispersion in fully developed turbulence, *Phys. Fluids*, *17*(11), 111701, doi:10.1063/1.2130751.

Boffetta, G., J. Davoudi, B. Eckhardt, and J. Schumacher (2004), Lagrangian tracers on a surface flow: The role of time correlations, *Phys. Rev. Lett.*, *93*, 134501, doi:10.1103/PhysRevLett.93.134501.

Castiglione, P., and A. Pumir (2001), Evolution of triangles in a two-dimensional turbulent flow, *Phys. Rev. E*, *64*, 56303, doi:10.1103/PhysRevE.64.056303.

Cressman, J. R., W. I. Goldburg, and J. Schumacher (2004a), Dispersion of tracer particles in a compressible flow, *Europhys. Lett.*, *66*(2), 219, doi:10.1209/epl/i2003-10187-x.

Cressman, J. R., J. Davoudi, W. I. Goldburg, and J. Schumacher (2004b), Eulerian and Lagrangian studies in surface flow turbulence, *New J. Phys.*, *6*(1), 53, doi:10.1088/1367-2630/6/1/053.

Crone, T. J., and M. Tolstoy (2010), Magnitude of the 2010 Gulf of Mexico oil leak, *Science*, *330*(6004), 634, doi:10.1126/science.1195840.

Davis, R. E. (1985), Drifter observations of coastal surface currents during CODE: The method and descriptive view, *J. Geophys. Res.*, *90*(C3), 4741–4755, doi:10.1029/JC090iC03p04741.

de Chaumont Quitry, A., D. H. Kelley, and N. T. Ouellette (2011), Mechanisms driving shape distortion in two-dimensional flow, *Europhys. Lett.*, *94*(6), 64006, doi:10.1209/0295-5075/94/64006.

Falkovich, G., K. Gawędzki, and M. Vergassola (2001), Particles and fields in fluid turbulence, *Rev. Mod. Phys.*, *73*, 913–975, doi:10.1103/RevModPhys.73.913.

Gawędzki, K., and M. Vergassola (2000), Phase transition in the passive scalar advection, *Physica D*, *138*(1–2), 63–90, doi:10.1016/S0167-2789(99)00171-2.

Huntley, H. S., B. L. Lipphardt, G. Jacobs, and A. D. Kirwan (2015), Clusters, deformation, and dilation: Diagnostics for material accumulation regions, *J. Geophys. Res. Oceans*, *120*, 6622–6636, doi:10.1002/2015JC011036.

Jacobs, G. A., H. S. Huntley, A. D. Kirwan, B. L. Lipphardt, T. Campbell, T. Smith, K. Edwards, and B. Bartels (2016), Ocean processes underlying surface clustering, *J. Geophys. Res. Oceans*, *121*, 180–197, doi:10.1002/2015JC011140.

Kalda, J., T. Soomere, and A. Giudici (2014), On the finite-time compressibility of the surface currents in the Gulf of Finland, the Baltic Sea, *J. Mar. Syst.*, *129*, 56–65, doi:10.1016/j.jmarsys.2012.08.010.

LaCasce, J. (2008), Statistics from Lagrangian observation, *Prog. Oceanogr.*, *77*(1), 1–29.

LaCasce, J. H., and C. Ohlmann (2003), Relative dispersion at the surface of the Gulf of Mexico, *J. Mar. Res.*, *61*(3), 285–312, doi:10.1357/002224003322201205.

Magome, S., T. Yamashita, T. Kohama, A. Kaneda, Y. Hayami, S. Takahashi, and H. Takeoka (2007), Jellyfish patch formation investigated by aerial photography and drifter experiment, *J. Oceanogr.*, *63*(5), 761–773, doi:10.1007/s10872-007-0065-y.

Mariano, A. J., et al. (2016), Statistical properties of the surface velocity field in the northern Gulf of Mexico sampled by GLAD drifters, *J. Geophys. Res. Oceans*, *121*, 5193–5216, doi:10.1002/2015JC011569.

Merrifield, S. T., D. H. Kelley, and N. T. Ouellette (2010), Scale-dependent statistical geometry in two-dimensional flow, *Phys. Rev. Lett.*, *104*, 254501, doi:10.1103/PhysRevLett.104.254501.

Molinari, R., and A. D. Kirwan (1975), Calculations of differential kinematic properties from Lagrangian observations in the Western Caribbean Sea, *J. Phys. Oceanogr.*, *5*(3), 483–491, doi:10.1175/1520-0485(1975)005<0483:CODKPF>2.0.CO;2.

Normile, D. (2014), Lost at sea, *Science*, *344*(6187), 963–965, doi:10.1126/science.344.6187.963.

Olascoaga, M. J., et al. (2013), Drifter motion in the Gulf of Mexico constrained by altimetric Lagrangian coherent structures, *Geophys. Res. Lett.*, *40*, 6171–6175, doi:10.1002/2013GL058624.

Özgökmen, T. M. (2012), CARTHE: GLAD experiment CODE-style drifter trajectories (lowpass filtered, 15 minute interval records), northern Gulf of Mexico near DeSoto Canyon, July–October 2012,Gulf of Mexico Research Initiative, doi:10.7266/N7VD6WC8. [Available at https://data.gulfresearchinitiative.org/data/R1.x134.073:0004.]

Poje, A. C. et al. (2014), Submesoscale dispersion in the vicinity of the Deepwater Horizon spill, *Proc. Natl. Acad. Sci. U.S.A.*, *111*(35), 12,693–12,698, doi:10.1073/pnas.1402452111.

Poulain, P., R. Gerin, E. Mauri, and R. Pennel (2009), Wind effects on drogued and undrogued drifters in the Eastern Mediterranean, *J. Atmos. Oceanic Technol.*, *26*(6), 1144–1156, doi:10.1175/2008JTECHO618.1.

Pumir, A., B. I. Shraiman, and M. Chertkov (2000), Geometry of Lagrangian dispersion in turbulence, *Phys. Rev. Lett.*, *85*, 5324–5327, doi:10.1103/PhysRevLett.85.5324.

Richardson, L. (1926), Atmospheric diffusion shown on a distance-neighborgraph, *Proc. R. Soc. A*, *11*, 709–737.

Rio, M.-H. (2010), Absolute dynamic topography from altimetry: Status and prospects in the upcoming GOCE Era, in *Oceanography from Space: Revisited*, edited by V. Barale, J. F. R. Gower, and L. Alberotanza, pp. 165–179, Springer, Netherlands, doi:10.1007/978-90-481-8681-5_10.

Rypina, I. I., S. R. Jayne, S. Yoshida, A. M. Macdonald, and K. Buesseler (2014), Drifter-based estimate of the 5 year dispersal of Fukushima-derived radionuclides, *J. Geophys. Res. Oceans*, *119*, 8177–8193, doi:10.1002/2014JC010306.

Saucier, W. J. (1955), *Principles of Meteorological Analysis*, Univ. of Chicago Press, Chicago.

Shcherbina, A. Y., E. A. D'Asaro, C. M. Lee, J. M. Klymak, M. J. Molemaker, and J. C. McWilliams (2013), Statistics of vertical vorticity, divergence, and strain in a developed submesoscale turbulence field, *Geophys. Res. Lett.*, *40*, 4706–4711, doi:10.1002/grl.50919.

Taylor, G. I. (1921), Diffusion by continuous movements, *Proc. London Math. Soc.*, *20*, 196–211.

Thiffeault, J.-L. (2005), Measuring topological chaos, *Phys. Rev. Lett.*, *94*, 084502, doi:10.1103/PhysRevLett.94.084502.

Yaremchuk, M., and E. Coelho (2014), Filtering drifter trajectories sampled at submesoscale resolution, *IEEE J. Oceanic Eng.*, *40*(3), 497–505, doi:10.1109/JOE.2014.2353472.

Zhong, Y., and A. Bracco (2013), Submesoscale impacts on horizontal and vertical transport in the Gulf of Mexico, *J. Geophys. Res. Oceans*, *118*, 5651–5668, doi:10.1002/jgrc.20402.